MISSOURI S&T

Missouri University of Science and Technology

Scholars' Mine

Materials Science and Engineering Faculty Research & Creative Works

Materials Science and Engineering

01 Jan 2013

Tailoring Spin-Orbit Torque in Diluted Magnetic Semiconductors

Hang Li

Xuhui Wang

Fatih Dogan
Missouri University of Science and Technology, doganf@mst.edu

Aurelien Manchon

Follow this and additional works at: https://scholarsmine.mst.edu/matsci_eng_facwork

Part of the Materials Science and Engineering Commons

Recommended Citation

Tailoring spin-orbit torque in diluted magnetic semiconductors

Hang Li, Xuhui Wang, Fatih Doğan, and Aurelien Manchon[a)]
King Abdullah University of Science and Technology (KAUST), Physical Science and Engineering Division, Thuwal 23955-6900, Saudi Arabia

We study the spin orbit torque arising from an intrinsic *linear* Dresselhaus spin-orbit coupling in a single layer III-V diluted magnetic semiconductor. We investigate the transport properties and spin torque using the linear response theory, and we report here: (1) a strong correlation exists between the angular dependence of the torque and the anisotropy of the Fermi surface; (2) the spin orbit torque depends nonlinearly on the exchange coupling. Our findings suggest the possibility to tailor the spin orbit torque magnitude and angular dependence by structural design. © 2013 AIP Publishing LLC.
[http://dx.doi.org/10.1063/1.4806981]

The electrical manipulation of magnetization is central to spintronic devices such as high density magnetic random access memory,[1] for which the spin transfer torque provides an efficient magnetization switching mechanism.[2,3] Beside the conventional spin-transfer torque, the concept of spin-orbit torque in both metallic systems and diluted magnetic semiconductors (DMS) has been studied theoretically and experimentally.[4–9] In the presence of a charge current, the spin-orbit coupling produces an effective magnetic field which generates a nonequilibrium spin density that, in turn, exerts a torque on the magnetization.[4–6] Several experiments on magnetization switching in strained (Ga,Mn)As have provided strong indications that such a torque can be induced by a Dresselhaus-type spin-orbit coupling, achieving critical switching currents as low as 10^6 A/cm².[7–9] However, up to date very few efforts are devoted to the nature of the spin-orbit torque in such a complex system, and its magnitude and angular dependence remain unaddressed.

In this letter, we study the spin-orbit torque in a diluted magnetic semiconductor submitted to a linear Dresselhaus spin-orbit coupling. We highlight two effects that have not been discussed before. First, a strong correlation exists between the angular dependence of the torque and the anisotropy of the Fermi surface. Second, the spin torque depends *nonlinearly* on the exchange coupling. To illustrate the flexibility offered by DMS in tailoring the spin-orbit torque, we compare the torques obtained in two stereotypical materials, (Ga,Mn)As and (In,Mn)As.

The system under investigation is a uniformly magnetized single domain DMS film made of, for example, (Ga,Mn)As or (In,Mn)As. We assume the system is well below its critical temperature. An electric field is applied along the $\hat{x}$ direction. It is worth pointing out that we consider here a large-enough system to allow us disregard any effects arising due to boundaries and confinement.

We use the *six-band* Kohn-Luttinger Hamiltonian to describe the band structure of the DMS[9]

$$H_{KL} = \frac{\hbar^2}{2m}\left[\left(\gamma_1 + \frac{5}{2}\gamma_2\right)k^2 - 2\gamma_3(\boldsymbol{k}\cdot\hat{\boldsymbol{J}})^2 + 2(\gamma_3 - \gamma_2)\sum_i k_i^2 \hat{J}_i^2\right],$$
(1)

[a)]aurelien.manchon@kaust.edu.sa

where the phenomenological Luttinger parameters $\gamma_{1,2,3}$ determine the band structure and the effective mass of valence-band holes. γ_3 is the anisotropy parameter, $\hat{\boldsymbol{J}}$ is the total angular momentum, and k is the wave vector. The bulk inversion asymmetry allows us to augment the Kohn-Luttinger Hamiltonian by a strain-induced spin-orbit coupling of the Dresselhaus type.[5,7] We assume the growth direction of (Ga,Mn)As is directed along the z-axis; two easy axes are pointed at x and y, respectively.[10] In this case, the components of the strain tensor ϵ_{xx} and ϵ_{yy} are identical. Consequently, we may have a linear Dresselhaus spin-orbit coupling[7]

$$H_{DSOC} = \beta(\hat{\sigma}_x k_x - \hat{\sigma}_y k_y),$$
(2)

given β the coupling constant that is a function of the axial strain.[7,11] $\hat{\sigma}_{x(y)}$ is the 6×6 spin matrix of holes and $k_{x(y)}$ is the wave vector.

In the DMS systems discussed here, we incorporate a mean-field like exchange coupling to enable the spin angular momentum transfer between the hole spin ($\hat{s} = \hbar\hat{\boldsymbol{\sigma}}/2$) and the localized ($d$-electron) magnetic moment $\hat{\boldsymbol{\Omega}}$ of ionized Mn²⁺ acceptors[12,13]

$$H_{ex} = 2J_{pd}N_{Mn}S_a\hat{\boldsymbol{\Omega}}\cdot\hat{s}/\hbar,$$
(3)

where J_{pd} is the antiferromagnetic coupling constant.[13,14] Here $S_a = 5/2$ is the spin of the acceptors. The hole spin operator, in the present six-band model, is a 6×6 matrix.[13] The concentration of the ordered local Mn²⁺ moments $N_{Mn} = 4x/a^3$ is given as a function of x that defines the doping concentration of Mn ion. a is the lattice constant. Therefore, the entire system is described by the total Hamiltonian

$$H_{sys} = H_{KL} + H_{ex} + H_{DSOC}.$$
(4)

In order to calculate the spin torque, we determine the nonequilibrium spin densities $\boldsymbol{S}$ (of holes) as a *linear* response to an external electric field[5]

$$\boldsymbol{S} = eE_x\frac{1}{V}\sum_{n,\boldsymbol{k}}\frac{1}{\hbar\Gamma_{n,\boldsymbol{k}}}\langle\hat{\boldsymbol{v}}\rangle\langle\hat{\boldsymbol{s}}\rangle\delta(E_{n,\boldsymbol{k}} - E_F),$$
(5)

where $\hat{v}$ is the velocity operator. In Eq. (5), the scattering rate of hole carriers by Mn ions is obtained by Fermi's golden rule[12]

$$\Gamma_{n,\mathbf{k}}^{Mn^{2+}} = \frac{2\pi}{\hbar} N_{Mn} \sum_{n'} \int \frac{d\mathbf{k}'}{(2\pi)^3} \left| M_{n,n'}^{\mathbf{k},\mathbf{k}'} \right|^2$$
$$\times \delta(E_{n,\mathbf{k}} - E_{n',\mathbf{k}'})(1 - \cos\phi_{\mathbf{k},\mathbf{k}'}), \qquad (6)$$

where $\phi_{\mathbf{k},\mathbf{k}'}$ is the angle between two wave vectors $\mathbf{k}$ and $\mathbf{k}'$. The matrix element $M_{n,n'}^{\mathbf{k},\mathbf{k}'}$ between two eigenstates $(\mathbf{k}, n)$ and $(\mathbf{k}', n')$ is

$$M_{n,n'}^{\mathbf{k}\mathbf{k}'} = J_{pd} S_a \langle \psi_{n\mathbf{k}} | \hat{\mathbf{\Omega}} \cdot \hat{\mathbf{s}} | \psi_{n'\mathbf{k}'} \rangle - \frac{e^2}{\epsilon(|\mathbf{k} - \mathbf{k}'|^2 + p^2)} \langle \psi_{n\mathbf{k}} | \psi_{n'\mathbf{k}'} \rangle. \qquad (7)$$

Here ϵ is the dielectric constant of the host semiconductors and $p = \sqrt{e^2 g/\epsilon}$ is the Thomas-Fermi screening wave vector, where g is the density of states at Fermi level. Finally, we calculate the field like spin-orbit torque using[4]

$$\mathbf{T} = J_{ex}\mathbf{S} \times \hat{\mathbf{\Omega}}, \qquad (8)$$

where $J_{ex} \equiv J_{pd}N_{Mn}S_a$. Throughout this letter, the results are given in terms of the torque efficiency $\mathbf{T}/eE$. The interband transitions, arising from distortions in the distribution function induced by the applied electric field, are neglected in our calculation. This implies that the torque extracted from the present model is expected to accommodate only a field-like component. The above protocols based on linear response formalism allow us to investigate the spin-orbit torque for a wide range of DMS material parameters.

We plot in Fig. 1(a) the spin torque as a function of the magnetization angle for different values of the band structure anisotropy parameter γ_3. The topology of the Fermi surface can be modified by a linear combination of γ_2 and γ_3: if $\gamma_2 = \gamma_3 \neq 0$, the Fermi surface around the Γ point is spherical, as shown in Fig. 1(c). In this special case, the angular dependence of the torque is simply proportional to $\cos\theta$ [red curve in Fig. 1(a)], as expected from the symmetry of the k-linear Dresselhaus Hamiltonian (Eq. (2)).[4] When $\gamma_3 \neq \gamma_2$, the Fermi surface deviates from a sphere [Figs. 1(b) and 1(d)], and, correspondingly, the angular dependence of the torque deviates from a simple $\cos\theta$ function [i.e., curves corresponding to $\gamma_3 = 1.0$ and $\gamma_3 = 2.93$ in Fig. 1(a)]. In a comparison to the spherical case, the maximal value of the torque at $\theta = 0$ is lower for $\gamma_3 \neq \gamma_2$. As Eq. (5) indicates, in the linear response treatment formulated here, the magnitude of the spin torque is determined by the transport scattering time and the expectation values of spin and velocity operators of holes. Qualitatively, as the Fermi surface deviates from a sphere, the expectation value $\langle \hat{s}_x \rangle$ of the heavy hole band, contributing the most to the spin torque, is lowered at $\theta = 0$.

More specifically, as the Fermi surface warps, the angular dependence of the spin torque develops, in addition to the $\cos\theta$ envelop function, an oscillation with a period that is shorter than π. The period of these additional oscillations increases as the Fermi surface becomes more anisotropic in k-space (see Figs. 1(b) and 1(d)). To further reveal the effect
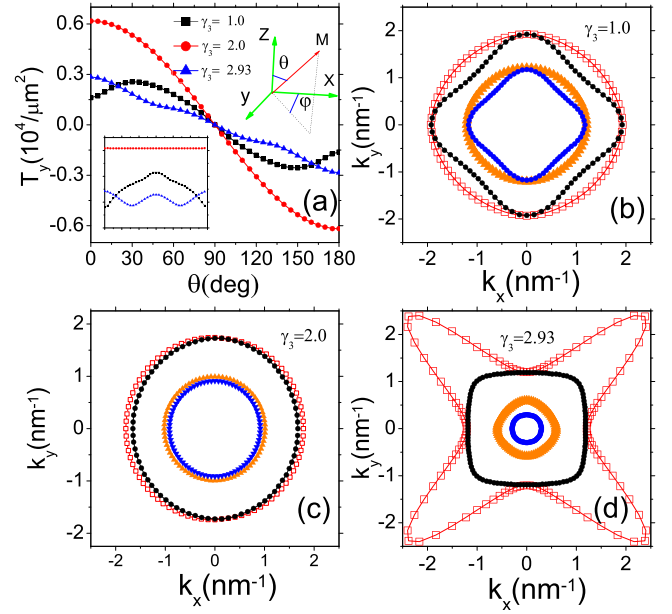

FIG. 1. (a) The y-component of the spin torque as a function of magnetization direction. Fermi surface intersection in the $k_z = 0$ plane for (b) $\gamma_3 = 1.0$, (c) $\gamma_3 = 2.0$, and (c) $\gamma_3 = 2.93$. The red, black, orange, and blue contours stand for majority heavy hole, minority heavy hole, majority light hole, and minority light hole band, respectively. Inset (a) depicts $T_y/\cos\theta$ as a function of magnetization direction. The other parameters are $(\gamma_1, \gamma_2) = (6.98, 2.0)$, $J_{pd} = 55\,\text{meV nm}^3$, and $p = 0.2\,\text{nm}^{-3}$.

of band warping on spin torque, we plot $T_y/\cos\theta$ as a function of the magnetization angle in inset of Fig. 1(a). When $\gamma_3 = 2.0$ (spherical Fermi sphere), $T_y/\cos\theta$ is a constant, for $T \propto \cos\theta$. When $\gamma_3 = 2.93$ or 1.0, the transport scattering time of the hole carriers starts to develop an oscillating behavior in θ,[15] which eventually contributes to additional angular dependencies in the spin torque. The angular dependencies in spin-orbit torque shall be detectable by techniques such as spin-ferromagnetic resonance (FMR).[9]

In Fig. 2, we compare the angular dependence of spin torque (T_y) for both (Ga,Mn)As and (In,Mn)As which are popular materials in experiments and device fabrication.[16–18] Although (In,Mn)As is, in terms of exchange coupling and general magnetic properties, rather similar to (Ga,Mn)As, the difference in band structures, lattice constants, and Fermi
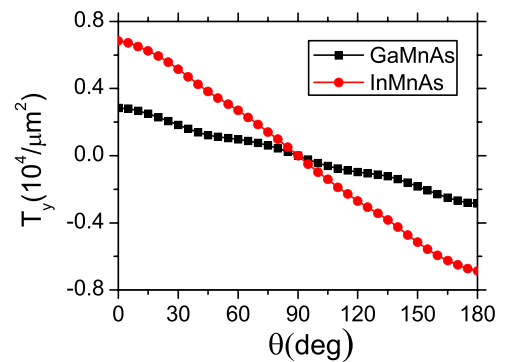

FIG. 2. Torque T_y as a function of the magnetization direction for (Ga,Mn)As (black square) and (In,Mn)As (red dots). For (Ga,Mn)As, $(\gamma_1, \gamma_2, \gamma_3) = (6.98, 2.0, 2.93)$; for (In,Mn)As, $(\gamma_1, \gamma_2, \gamma_3) = (20.0, 8.5, 9.2)$. The strength of the spin-orbit coupling constant is for (Ga,Mn)As, $\beta = 1.6\,\text{meV nm}$; for (In,Mn)As, $\beta = 3.3\,\text{meV nm}$.[19] The exchange coupling constant $J_{pd} = 55\,\text{meV nm}^3$ for (Ga,Mn)As (Ref. 20) and 39 meV nm^3 for (In,Mn)As.[21]

energies between these two materials gives rise to different density of states, strains, and transport scattering rates. For both materials, the spin torque decreases monotonically as the angle θ increases from 0 to $\pi/2$. Throughout the entire angle range $[0, \pi]$, the amplitude of the torque in (In,Mn)As is twice larger than that in (Ga,Mn)As. We mainly attribute this to two effects. First of all, the spin-orbit coupling constant β in (In,Mn)As is about twice larger than that in (Ga,Mn)As. Second, for the same hole concentration, the Fermi energy of (In,Mn)As is higher than that of (Ga,Mn)As.

In the following, we further demonstrate a counter-intuitive feature that in the DMS system considered in this letter, the spin orbit torque depends nonlinearly on the exchange splitting. In Fig. 3(a), T_y component of the spin torque is plotted as a function of the exchange coupling J_{pd}, for different values of β. In the weak exchange coupling regime, the electric generation of non equilibrium spin density dominates, and then the leading role of exchange coupling is defined by its contribution to the transport scattering rate. We provide a simple qualitative explanation on such a peculiar J_{pd} dependence. Using a Born approximation, the scattering rate due to the p–d interaction is proportional to $1/\tau_J = bJ_{pd}^2$, where parameter b is J_{pd}- independent. When the nonmagnetic scattering rate $1/\tau_0$ is taken into account, i.e., the Coulomb interaction part in Eq. (7), the total scattering time in Eq. (5) can be estimated as

$$\frac{1}{\hbar\Gamma} \propto \frac{1}{bJ_{pd}^2 + \frac{1}{\tau_0}}, \qquad (9)$$

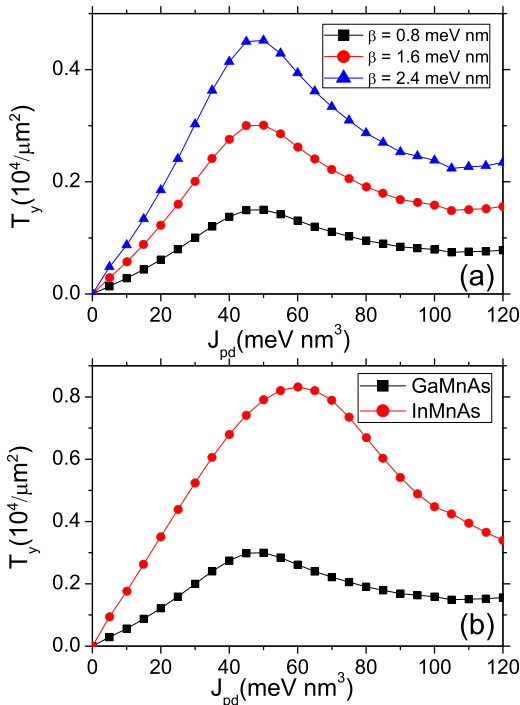which contributes to the torque by $T \propto J_{pd}/(\hbar\Gamma)$. This explains the transition behavior, i.e., increases linearly then decreases, in the moderate J_{pd} regime in Fig. 3. As the exchange coupling further increases, Eq. (9) is dominated by the spin-dependent scattering; therefore, the scattering time $1/\hbar\Gamma \propto 1/J_{pd}^2$. Meanwhile, the energy splitting due to the exchange coupling becomes significant; thus, $\langle \hat{s} \rangle \propto J_{pd}$. In total, the spin torque is insensitive to J_{pd}, explaining the flat curve in the large exchange coupling regime. In Fig. 3(b), we plot the influence of the exchange coupling on the spin torque for two materials. In (In,Mn)As, mainly due to a larger Fermi energy in a comparison to (Ga,Mn)As, the peak of the spin torque shifts towards a larger J_{pd}. The dependence of the torque as a function of the exchange in (In,Mn)As is more pronounced than in (Ga,Mn)As, due to a stronger spin-orbit coupling.

The possibility to engineer electronic properties by doping is one of the defining features that make DMS promising for applications. Here, we focus on the doping effect which allows the spin torque to vary as a function of hole carrier concentration. In Fig. 4(a), the torque is plotted as a function of the hole concentration for different β parameters. With the increase of the hole concentration, the torque increases due to an enhanced Fermi energy. In the weak spin-orbit coupling regime (small β), the torque as a function of the hole concentration (p) follows roughly the $p^{1/3}$ curve as shown in the inset in Fig. 4(a). The spherical Fermi sphere approximation and a simple parabolic dispersion relation allow for an analytical expression of the spin torque, i.e., in the leading order in β and J_{ex},

$$T = \frac{m^*}{\hbar} \frac{\beta J_{ex}}{E_F} \sigma_D, \qquad (10)$$

FIG. 3. The T_y component of the spin torque as a function of exchange coupling J_{pd}. (a) T_y versus J_{pd} at various values of β, for (Ga,Mn)As. (b) T_y versus J_{pd}, for both (Ga,Mn)As and (In,Mn)As. The magnetization is directed along the z-axis ($\theta = 0$). The other parameters are the same as those in Fig. 2.
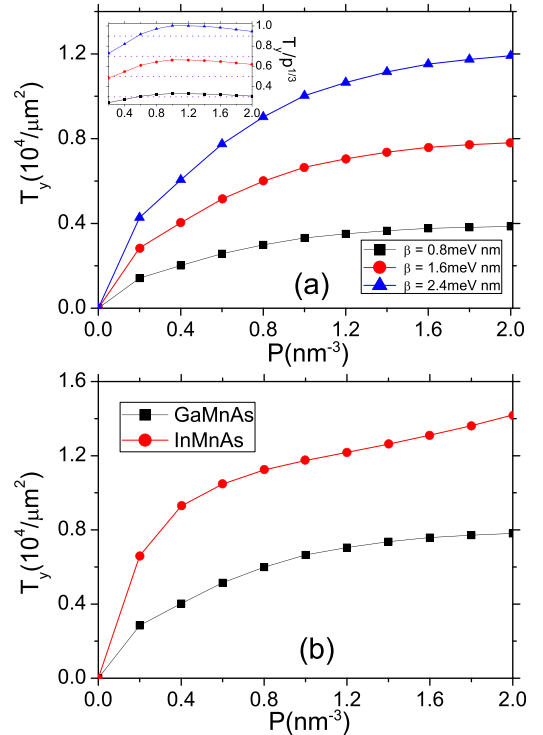

FIG. 4. The y-component of the spin torque as a function of hole concentration. (a) The y-component of the spin torque versus hole concentration at different β. (b) Spin torque versus hole concentration in (Ga,Mn)As and (In,Mn)As. For (Ga,Mn)As, $J_{pd} = 55 \, \text{meV} \, \text{nm}^3$; for (In,Mn)As, $J_{pd} = 39 \, \text{meV} \, \text{nm}^3$. The other parameters are the same as in Fig. 3.

where m^* is the effective mass. The Fermi energy E_F and the Drude conductivity are given by

$$E_F = \frac{\hbar^2}{2m^*}(3\pi^2 p)^{2/3}, \quad \sigma_D = \frac{e^2\tau}{m^*}p, \tag{11}$$

where τ is the transport time. The last two relations immediately give rise to $T \propto p^{1/3}$. In the six-band model, the Fermi surface deviates from a sphere and, as the value of β increases, the spin-orbit coupling starts to modify the density of states. Both effects render the torque-versus-hole concentration curve away from the $p^{1/3}$ dependence. This effect is illustrated in Fig. 4(b). The former (strong spin-orbit coupling) clearly deviates from $p^{1/3}$, whereas the latter (weak spin-orbit coupling) follows the expected $p^{1/3}$ trend.

In conclusion, in a DMS system subscribing to a linear Dresselhaus spin-orbit coupling, we have found that the angular dependence of the spin-orbit torque has a strong yet intriguing correlation with the anisotropy of the Fermi surface. Our study also reveals a nonlinear dependence of the spin torque on the exchange coupling. From the perspective of material selection, for an equivalent set of parameters, the critical switching current needed in (In,Mn)As is expected to be lower than that in (Ga,Mn)As. The results reported here shed light on the design and applications of spintronic devices based on DMS.

While the materials studied in this work have a Zinc-Blende structure, DMS adopting a wurtzite structure, such as (Ga,Mn)N, might also be interesting candidates for spin-orbit torque observation due to their sizable bulk Rashba spin-orbit coupling. However, these materials usually present a significant Jahn-Teller distortion that is large enough to suppress the spin-orbit coupling.[22] Furthermore, the formalism developed here applies to systems possessing delocalized holes and long range Mn-Mn interactions and is not adapted to the localized holes controlling the magnetism in (Ga,Mn)N.

[1] J. A. Katine, F. J. Albert, R. A. Buhrman, E. B. Myers, and D. C. Ralph, Phys. Rev. Lett. **84**, 3149 (2000).
[2] J. Slonczewski, J. Magn. Magn. Mater. **159**, L1 (1996).
[3] L. Berger, Phys. Rev. B **54**, 9353 (1996).
[4] A. Manchon and S. Zhang, Phys. Rev. B **78**, 212405 (2008); **79**, 094422 (2009).
[5] I. Garate and A. H. MacDonald, Phys. Rev. B **80**, 134403 (2009).
[6] K. M. D. Hals, A. Brataas, and Y. Tserkovnyak, Eur. Phys. Lett. **90**, 47002 (2010).
[7] A. Chernyshov, M. Overby, X. Liu, J. K. Furdyna, Y. Lyanda-Geller, and L. P. Rokhinson, Nat. Phys. **5**, 656 (2009).
[8] M. Endo, F. Matsukura, and H. Ohno, Appl. Phys. Lett. **97**, 222501 (2010).
[9] D. Fang, H. Kurebayashi, J. Wunderlich, K. Výborný, L. P. Zârbo, R. P. Campion, A. Casiraghi, B. L. Gallagher, T. Jungwirth, and A. J. Ferguson, Nat. Nanotechnol. **6**, 413 (2011).
[10] U. Welp, V. K. Vlasko-Vlasov, X. Liu, J. K. Furdyna, and T. Wojtowicz, Phys. Rev. Lett. **90**, 167206 (2003).
[11] B. A. Bernevig and S.-C. Zhang, Phys. Rev. B **72**, 115204 (2005).
[12] T. Jungwirth, M. Abolfath, J. Sinova, J. Kučera, and A. H. MacDonald, Appl. Phys. Lett. **81**, 4029 (2002).
[13] M. Abolfath, T. Jungwirth, J. Brum, and A. H. MacDonald, Phys. Rev. B **63**, 054418 (2001).
[14] J. van Bree, P. M. Koenraad, and J. Fernández-Rossier, Phys. Rev. B **78**, 165414 (2008).
[15] A. W. Rushforth, K. Výborný, C. S. King, K. W. Edmonds, R. P. Campion, C. T. Foxon, J. Wunderlich, A. C. Irvine, P. Vašek, V. Novák, K. Olejník, J. Sinova, T. Jungwirth, and B. L. Gallagher, Phys. Rev. Lett. **99**, 147207 (2007).
[16] H. Ohno, H. Munekata, T. Penney, S. von Molnár, and L. L. Chang, Phys. Rev. Lett. **68**, 2664 (1992).
[17] S. Koshihara, A. Oiwa, M. Hirasawa, S. Katsumoto, Y. Iye, C. Urano, H. Takagi, and H. Munekata, Phys. Rev. Lett. **78**, 4617 (1997).
[18] T. Jungwirth, Q. Niu, and A. H. MacDonald, Phys. Rev. Lett. **88**, 207208 (2002).
[19] J. Fabian, A. Matos-Abiague, C. Ertler, P. Stano, and I. Žutić, Acta Phys. Slov. **57**, 565 (2010).
[20] H. Ohno, J. Magn. Magn. Mater. **200**, 110 (1999).
[21] J. Wang, Master's thesis, Rice University, Houston, Texas, 2002.
[22] A. Stroppa and G. Kresse, Phys. Rev. B **79**, 201201 (2009).